Model Based Predictive Control for a Solar-Thermal System

Tarik Ferhatbegović, Gerhard Zucker and Peter Palensky
Austrian Institute of Technology
Energy Department
Vienna, Austria
Email: {tarik.ferhatbegovic.fl, gerhard.zucker, peter.palensky}@ait.ac.at

***Abstract*—Buildings and their components account for a major amount of the overall global energy consumption. There is a rising demand to increase the end-use energy efficiency. Advanced automation and control for buildings and their components is one possibility how to achieve the desired goal of lower energy consumption. The model based predictive control approach as a special form of optimal control offers a good way to increase energy efficiency. This paper presents the employment of a model based predictive control algorithm for the energy efficient temperature control of a solar-thermal system consisting of a solar collector and a heat exchanger. The design of the controller is based upon a physical lumped model of the system components. In order to illustrate the potential of the model predictive approach for the use in building automation the comparison to a standard PI control approach is made where the energy consumption for both control concepts is analyzed.**

I. Introduction

Around 40% of the global total energy consumption is allocated to buildings [1]. Heating, ventilation and air-conditioning systems (HVAC) account for approx. 50% of the energy end use in residential and non-residential buildings [2]. The reduction of the energy consumption yields a substantial decrease of greenhouse emissions and therefore contributes to the required climate change mitigation [3]. The employment of established passive technologies such as improved building insulations or more energy efficient appliances for heating and cooling are efficient methods towards the energy efficient operation of buildings. Another approach to mitigate climate change is to improve buildings' automation by using advanced control concepts [1].

Current implementations of control concepts in buildings are still very modest, often pursuing rule-based approaches combined with PID controllers. Hereby, set-points for the control are mostly determined based on schedules or plans, rather than being the output of an optimization algorithm, neither taking into account the efficiency of the consumed energy, nor considering relevant system constraints (e.g.: temperature limits, comfort, etc.).

Model based predictive control (MBPC) offers a good possibility to employ energy efficient control for buildings and building components on the one hand and to deal with the slow thermal dynamics as well as time delays in buildings on the other hand. Though it has been the elected control scheme in many research areas, in particular for mechanical, electrical or chemical systems (see e.g.: [4], [5] or [6]), its use in building research is relatively still very rare. However, the benefits of MBPC have attracted attention of many researchers in building engineering, therefore increasing its popularity rapidly.

For instance the authors in [7] deal with the model based predictive control approach for temperature control in buildings, where the future behavior of the process is predicted based upon a system model. The approach is compared to a standard concept using PI controllers. In [8] stochastic weather predictions are used for the employment of model predictive controllers where the study is carried out for different buildings variants under different weather conditions. The work [9] addresses the use of model based predictive control in combination with a distributed approach for the multizone building temperature regulation for which a communication between the individual controllers is established. Some other works consider the use of fuzzy model predictive control [10] or model based predictive control employing neural networks [11].

In this study, a mathematical state-space model for the solar-thermal system implemented in the ENERGYbase [12], which is an office building meeting the passive house standards, is developed. Based on the information about the system dynamics, a discrete model predictive controller is implemented and tested for robustness including information about weather changes (e.g.: ambient temperature, solar radiation, etc.) which is modeled in terms of disturbance rejection. For the components of the solar-thermal system including the solar collector field as well as the heat-exchanger, object-oriented modeling using the open source modeling language Modelica [13] and validation of the models have been carried out in [14] and [15]. The aim is to control the temperature at the outputs of the heat exchanger in the solar circuit as well as storage circuit using model based predictive control where the desired set-points for the temperature should be achieved predictively consuming the minimum of energy whereas variations of (e.g.: solar radiation, ambient temperature, etc.) should be rejected.

II. Physical Modeling of the Solar-Thermal System

In this section a mathematical model of the solar-thermal system using fundamental balance laws such as the energy balance equations for thermal systems will be derived. The

model should be composed such that the approach towards the design of the model predictive controller is carried out in a systematic way. The system dynamics are represented by state vectors providing the current system information required for predicting ahead. Fig. 1 depicts the structure of the solar thermal system considered in this study for which temperature control is pursued.

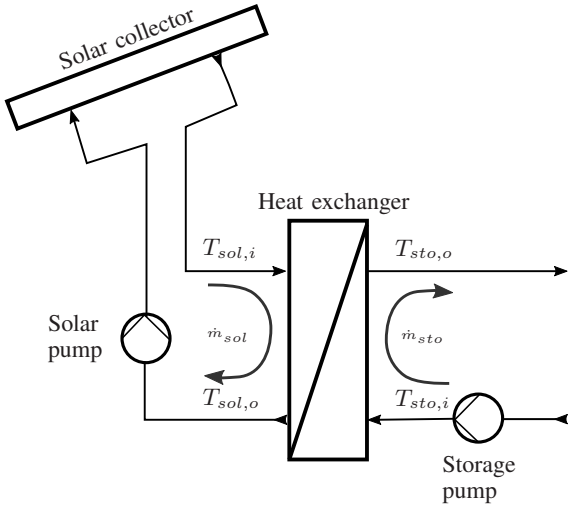

Fig. 1: Structure of the Solar Thermal System.

Fig. 2 shows the structure of the proposed control concept. The model based predictive controller consists of a physical model of the controlled system as well as an objective function together with constraints for which the optimization routine yields the desired control law. The variables $T^*_{sol,o}$ and $T^*_{sto,o}$ denote the desired output temperatures in the solar and storage circuit respectively. T_{amb} which represents the ambient temperature of the solar thermal system and G_t accounting for the solar radiation are considered as disturbances by the controller and therefore subject to rejection control. $\dot{m}_{sol}$ and $\dot{m}_{sto}$ serve as the manipulated variables of the closed-loop control.

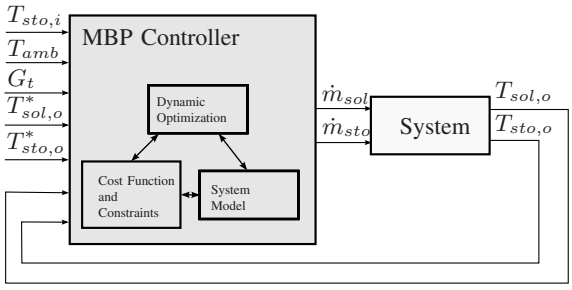

Fig. 2: Block Diagram of the Control Structure.

A. Heat Exchanger Model

In this section a state space model of the counter current flow plate heat exchanger suitable for the design of the model predictive controller is developed. For that purpose the heat exchanger is modeled using the approach of early lumping of the plant, see [16] and [17]. Hereby N ideally mixed interconnected tanks are used, which is illustrated by Fig. 3.

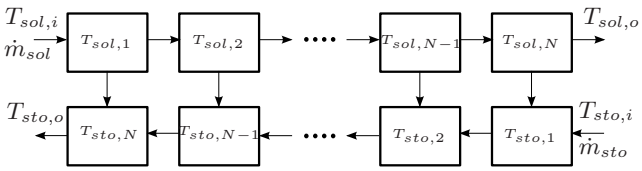

Fig. 3: Lumped Model of the Heat Exchanger.

The model represents the dynamic behavior of the heat exchanger accurately also taking into account the nonlinearities arising from the heat transfer due to the mass flow rates as well as the temperature states. For simulation purposes we aim at a model with a higher number N of the tanks. However, to keep the controller design simple, we will use a second order system for the heat exchanger dynamics in order to design the predictive controller, therefore $N = 2$. Thereby, the following assumptions are made prior to the modeling of the system components:

- The medium considered for heating is incompressible.
- The medium density as well as its viscosity are considered constant.
- The thermal inertia of the medium in the pipes is neglected.
- There is no heat loss to the ambient.

The heat exchanger dynamics can thus be described using Equations 1 and 2 representing the energy flow inside the heat exchanger.

$$\frac{\mathrm{d}}{\mathrm{d}t}T_{sol,o} = \frac{1}{M_h c_h}(\dot{m}_{sol}\,(T_{sol,i} - T_{sol,o}) - A_h U \Delta T_{mean}) \tag{1}$$

$$\frac{\mathrm{d}}{\mathrm{d}t}T_{sto,o} = \frac{1}{M_c c_c}(\dot{m}_{sto}\,(T_{sto,i} - T_{sto,o}) + A_c U \Delta T_{mean}) \tag{2}$$

The term $A_s U \Delta T_{mean}$ with $s \in [h, c]$ refers to the transfer of heat between the hot and the cold lumps whereas the variable U describes the overall heat transfer coefficient which will be considered constant over time for the design of the controller. For simulation purposes to test the controller it will be kept as a function of the mass flow rates and therefore be time-dependent. ΔT_{mean} which corresponds to the logarithmic mean temperature difference can be expressed by (3) as shown in [18] and [19].

$$\Delta T_{mean} = \frac{T_{sol,i} + T_{sto,i} - T_{sto,o} - T_{sol,o}}{\ln \frac{T_{sol,i} - T_{sto,o}}{T_{sol,o} - T_{sto,i}}} \tag{3}$$

For our controller design as well as for simulation purposes we will use an algebraic approximation of the term describing the temperature difference ΔT_{mean} according to [18], see (4).

$$\Delta T_{mean} = \frac{1}{2}\left(T_{sol,i} + T_{sol,o}\right) - \frac{1}{2}\left(T_{sto,i} + T_{sol,o}\right) \tag{4}$$

B. Solar Collector Model

Solar collectors belong to the class of heat exchangers which convert solar radiation to internal energy of the transported heating medium [20]. In this subsection a transient model for the solar collector suitable for the design of the model predictive controller is developed. The solar thermal system implemented in the ENERGYbase comprises a glass-covered flat plate solar collector field with a total aperture area of 274m^2 [14].

The steady-state behavior of a flat plate solar collector can be easily described using its efficiency, see (5).

$$\eta = c_0 - c_1 \frac{T_{sol,i} - T_{amb}}{G_{tot}} - c_2 \frac{(T_{sol,i} - T_{amb})^2}{G_{tot}} \tag{5}$$

Here c_0, c_1 as well as c_2 denote parameters which are dependent on the optical performances as well as the heat loss properties of the solar collector field. G_{tot} represents the total specific energy gain by radiation and can be calculated as a function of the diffusive and the beam solar radiation. T_{amb} denotes the ambient temperature.

By knowing the total aperture area of the solar collector A_c field and using the solar collector efficiency from (5), the total heat flow rate $\dot{Q}_{col}$ for the heating medium at the outlet of the solar collector field can be calculated according to (6).

$$\dot{Q}_{col} = \eta \; A_c \; G_{tot} \tag{6}$$

In order to obtain the information about the transient behavior of the outlet temperature $T_{sol,i}$ of the solar collector panel which is the inlet temperature of the solar circuit of the heat exchanger, we apply the energy balance at the level of the absorber plate:

$$\frac{\mathrm{d}}{\mathrm{d}t} T_{sol,i} = \frac{1}{c_{dyn}} (\dot{Q}_{col} + \dot{m}_{sol} c_p \left(T_{sol,o} - T_{sol,i}\right)) \tag{7}$$

using c_{dyn} as the dynamic heat capacity of the solar collector panel. c_p describes the specific heat capacity of the heating medium. $\dot{Q}_{col}$ is taken from (6) whereas the collector efficiency is provided by (5).

C. Total Solar Thermal System Model

For the subsequent controller design the overall model is given using state-space formulation:

$$\begin{aligned} \dot{\mathbf{x}} &= \mathbf{f}\left(\mathbf{x}\right) + \mathbf{g}\left(\mathbf{x}\right)\mathbf{u} \\ \mathbf{y} &= \mathbf{h}\left(\mathbf{x}\right) \end{aligned} \tag{8}$$

with the state vector $\mathbf{x} = [T_{sol,o}, T_{sto,o}, T_{sol,i}]^{\mathrm{T}}$ and the output vector $\mathbf{y} = [T_{sol,o}, T_{sto,o}]^{\mathrm{T}}$ as well as the affine input $\mathbf{u} = [\dot{m}_{sol}, \dot{m}_{sto}]$ which yields for the solar thermal system from Fig. 1 the following structure:

$$\begin{bmatrix} \frac{\mathrm{d}}{\mathrm{d}t} T_{sol,o} \\ \frac{\mathrm{d}}{\mathrm{d}t} T_{sto,o} \\ \frac{\mathrm{d}}{\mathrm{d}t} T_{sol,i} \end{bmatrix} = \begin{bmatrix} \frac{1}{M_h c_h}(\dot{m}_{sol}\left(T_{sol,i} - T_{sol,o}\right) - A_h U \Delta T_{mean}) \\ \frac{1}{M_c c_c}(\dot{m}_{sto}\left(T_{sto,i} - T_{sto,o}\right) + A_c U \Delta T_{mean}) \\ \frac{1}{c_{dyn}}(A_c(c_0 \; G_{tot} - c_1(T_{sol,i} - T_{amb}) \\ -c_2(T_{sol,i} - T_{amb})^2) \\ +\dot{m}_{sol} c_p \left(T_{sol,o} - T_{sol,i}\right)) \end{bmatrix} \tag{9}$$

by using (4) to express ΔT_{mean}.

III. Model Based Predictive Controller Design

In this section the model predictive controller for the solar thermal system from Fig. 1 is developed. As the control task is to control the outlet temperatures of the heat exchanger in a small region around a defined operating point, we will carry out the linearization of the nonlinear controlled system from (9) at the defined operating point. As the control algorithm is implemented in discrete form, the discrete state space representation for the linearized model reads as provided by (10).

$$\begin{aligned} \mathbf{x}(k+1) &= \Phi \mathbf{x}(k) + \mathbf{\Gamma} \mathbf{u}(k) + \mathbf{\Lambda} \mathbf{w}(k) \\ \mathbf{y}(k) &= C \mathbf{x}(k) \end{aligned} \tag{10}$$

The vector $\mathbf{u}(k)$ contains the mass flow rates $[\dot{m}_{sol}(k), \dot{m}_{sto}(k)]^{\mathrm{T}}$ used as the control variables for temperature control of the solar thermal system. The states are represented by the vector $\mathbf{x}(k) = [T_{sol,o}(k), T_{sto,o}(k), T_{sol,i}(k)]^{\mathrm{T}}$ considering the current time instant k. Furthermore, (10) comprises an additional term $\mathbf{\Lambda \omega(k)}$ for which the matrix $\mathbf{\Lambda}$ contains the local transient information about disturbances together with the vector $\boldsymbol{\omega}(k) = [G_{tot}, T_{amb}, T_{sto,i}]^{\mathrm{T}}$ denoting the radiation, the ambient temperature and the inlet temperature in the storage circuit. Therefore, disturbances due to weather changes can be rejected predictively, hence keeping the temperature at the desired comfort level. The matrices $\mathbf{\Phi}$ and $\mathbf{\Gamma}$ contain the discrete linearized information about the states $\mathbf{x}(k)$ and the inputs $\mathbf{u}(k)$ in a small region around the operating point.

The predictive feature of the model predictive controller demands the use of a dynamic model of the system to be controlled where the prediction is carried out during a finite time horizon relying on the past input and output signals as well as the signals to be computed. The control law generated by the model predictive controller is based on iterative optimization of the system model. At the current time instant k the system is sampled and an optimal control strategy is calculated by minimizing a defined cost function. Usually, the receding horizon principle is employed for which only the first step of the control law calculated for the entire control horizon N_c is applied to the system model. At the next sample instant $k+1$

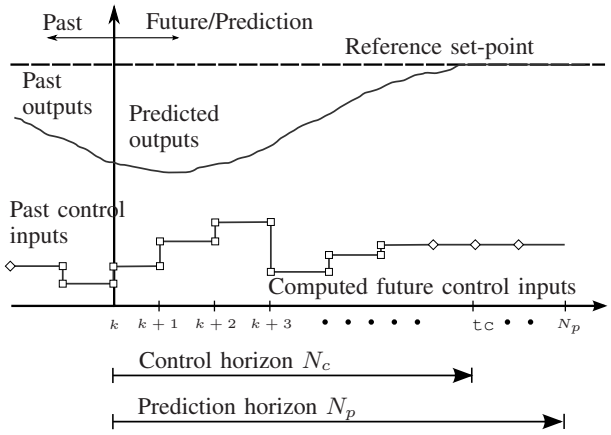

Fig. 4: The Principle of Model Predictive Control.

the optimization is redone, resulting in a new control law and new predicted state trajectories. Fig. 4 illustrates the principle of model predictive control.

For the temperature control problem at hand we propose a quadratic cost function which fulfills the criteria of optimality with regards to the energy consumption as well as the minimization of the control error $\mathbf{y}^*(k) - \mathbf{y}(k)$, see (11).

$$\min_{\mathbf{\Delta u}} J := \sum_{i=0}^{N_p} \delta_y(i) \left[\mathbf{y}^*(k+i) - \mathbf{y}(k+i)\right]^2 + \sum_{i=0}^{N_c} \delta_u(i) \left[\mathbf{u}(k+i)\right]^2 \tag{11}$$

subject to

$$\begin{aligned} \mathbf{u}_{min} &\leq \mathbf{u}(k) \leq \mathbf{u}_{max} \\ \mathbf{\Delta u}_{min} &\leq \mathbf{\Delta u}(k) \leq \mathbf{\Delta u}_{max} \\ \mathbf{y}_{min} &\leq \mathbf{y}(k) \leq \mathbf{y}_{max} \end{aligned}$$

$\mathbf{y}^*(k)$ denotes the desired trajectory at the current time instant k. The constraints put on the control variables $\mathbf{u}(k)$, the control increments $\mathbf{\Delta u}(k)$ as well as the outputs $\mathbf{y}(k)$ must be satisfied at any time instant k during the optimization routine. The second term from (11) accounts for the minimization of the energy consumed by the pumps in the solar as well as the storage circuit.

As our aim is to minimize the cost function with regards to the control increment $\mathbf{\Delta u}(k)$ by applying a quadratic programming algorithm, the optimization problem from (11) is rewritten which results in the form provided in (12) whereas the constraints from (11) remain the same.

$$\min_{\mathbf{\Delta u}} J := \sum_{i=0}^{N_p} \delta_y(i) \left[\mathbf{y}^*(k+i) - \mathbf{y}(k+i)\right]^2 + \sum_{i=0}^{N_c} \delta_u(i) \left[\mathbf{\Delta u}(k+i) + \mathbf{u}(k+i-1)\right]^2 \tag{12}$$

Hence, for the purpose of implementation using the optimization algorithm the cost function J can be given in matrix notation as provided by (13).

$$\begin{aligned} J = &\left(\mathbf{Y}^* - \mathbf{Y}\right)^{\mathrm{T}} \boldsymbol{\lambda}_y \left(\mathbf{Y}^* - \mathbf{Y}\right) \\ &+ \left(\mathbf{\Delta U} + \mathbf{U}_\pi\right)^{\mathrm{T}} \boldsymbol{\lambda}_u \left(\mathbf{\Delta U} + \mathbf{U}_\pi\right) \end{aligned} \tag{13}$$

where $\boldsymbol{\lambda}_y > 0$ and $\boldsymbol{\lambda}_u > 0$ denote positive definite weighting matrices.

Defining the vectors

$$\begin{aligned} \mathbf{Y}^* &= [\mathbf{y}^*(k_i), \mathbf{y}^*(k_i+1), \ldots, \mathbf{y}^*(k_i+N_p)] \\ \mathbf{Y} &= [\mathbf{y}(k_i), \mathbf{y}(k_i+1), \ldots, \mathbf{y}(k_i+N_p)] \\ \mathbf{\Delta U} &= [\Delta\mathbf{u}(k_i), \Delta\mathbf{u}(k_i+1), \ldots, \Delta\mathbf{u}(k_i+N_c-1)] \\ \mathbf{U}_\pi &= [\mathbf{u}(k_i-1), \mathbf{u}(k_i), \mathbf{u}(k_i+1) \ldots, \mathbf{u}(k_i+N_c-2)] \end{aligned} \tag{14}$$

where $\mathbf{Y}^*$ contains the desired values from the reference trajectory and $\mathbf{Y}$ comprises the actual output trajectory for each output and $\mathbf{U}_\pi$ represents a vector with control variable values from the previous optimization iteration for each input and output of the MIMO (multiple-input/multiple-output) system from (9).

The trajectory of the output $\mathbf{Y}$ can be expressed using the following (15).

$$\mathbf{Y} = \mathbf{F}\mathbf{x}(k_i) + \mathbf{\Phi_u}\mathbf{\Delta U} + \mathbf{\Phi}_\omega\mathbf{\Delta\omega} \tag{15}$$

where

$$\mathbf{F} = \begin{bmatrix} \mathbf{C\Phi} \\ \mathbf{C\Phi}^2 \\ \mathbf{C\Phi}^3 \\ \vdots \\ \mathbf{C\Phi}^{N_p} \end{bmatrix}, \tag{16}$$

$$\mathbf{\Phi_u} = \begin{bmatrix} \mathbf{C\Gamma} & \mathbf{0} & \cdots & \mathbf{0} \\ \mathbf{C\Phi\Gamma} & \mathbf{C\Gamma} & \cdots & \mathbf{0} \\ \mathbf{C\Phi}^2\mathbf{\Gamma} & \mathbf{C\Phi\Gamma} & \cdots & \mathbf{0} \\ \vdots & & & \\ \mathbf{C\Phi}^{N_p-1}\mathbf{\Gamma} & \mathbf{C\Phi}^{N_p-2}\mathbf{\Gamma} & \cdots & \mathbf{C\Phi}^{N_p-N_c}\mathbf{\Gamma} \end{bmatrix},$$

$$\mathbf{\Phi}_\omega = \begin{bmatrix} \mathbf{C\Lambda} & \mathbf{0} & \cdots & \mathbf{0} \\ \mathbf{C\Phi\Lambda} & \mathbf{C\Lambda} & \cdots & \mathbf{0} \\ \mathbf{C\Phi}^2\mathbf{\Lambda} & \mathbf{C\Phi\Lambda} & \cdots & \mathbf{0} \\ \vdots & & & \\ \mathbf{C\Phi}^{N_p-1}\mathbf{\Lambda} & \mathbf{C\Phi}^{N_p-2}\mathbf{\Lambda} & \cdots & \mathbf{C\Lambda} \end{bmatrix}$$

and the vector $\mathbf{\Delta\omega} = [\boldsymbol{\omega}(k_i), \boldsymbol{\omega}(k_i+1), \ldots, \boldsymbol{\omega}(k_i+N_p)]$ contains the predicted disturbances for the prediction horizon N_p.

Inserting (15) into (12) the cost function J becomes a function of the future control increments $\mathbf{\Delta U}$ and the current states $\mathbf{x}(k_i)$, see (17).

$$J\left(\boldsymbol{\Delta}\mathbf{U},\mathbf{x}(k_i)\right) = \left(\mathbf{Y}^* - \mathbf{F}\mathbf{x}(k_i) - \boldsymbol{\Phi}_\mathbf{u}\boldsymbol{\Delta}\mathbf{U} - \boldsymbol{\Phi}_\omega\boldsymbol{\Delta}\boldsymbol{\omega}\right)^{\mathrm{T}} \boldsymbol{\lambda}_y \left(\mathbf{Y}^* - \mathbf{F}\mathbf{x}(k_i) - \boldsymbol{\Phi}_\mathbf{u}\boldsymbol{\Delta}\mathbf{U} - \boldsymbol{\Phi}_\omega\boldsymbol{\Delta}\boldsymbol{\omega}\right) + \left(\Delta\mathbf{U} + \mathbf{U}_\pi\right)^{\mathrm{T}} \boldsymbol{\lambda}_u \left(\Delta\mathbf{U} + \mathbf{U}_\pi\right) \quad (17)$$

The optimal sequence $\boldsymbol{\Delta}\mathbf{U}$ is calculated by solving the quadratic programming problem provided by (18) in combination with the constraints from (11).

$$\min_{\boldsymbol{\Delta}\mathbf{U}} \frac{1}{2}\boldsymbol{\Delta}\mathbf{U}^{\mathrm{T}}\boldsymbol{\mathcal{H}}\boldsymbol{\Delta}\mathbf{U} + \mathcal{F}^{\mathrm{T}}\boldsymbol{\Delta}\mathbf{U} \quad (18)$$

where

$$\boldsymbol{\mathcal{H}} = 2{\boldsymbol{\Phi}_\mathbf{u}}^{\mathrm{T}}\boldsymbol{\lambda}_y\boldsymbol{\Phi}_\mathbf{u} + 2\boldsymbol{\lambda}_u \quad (19)$$

denotes the Hessian matrix and

$$\mathcal{F}^{\mathrm{T}} = -2{\boldsymbol{\Phi}_\mathbf{u}}^{\mathrm{T}}\boldsymbol{\lambda}_y\left(\mathbf{Y}^* - \mathbf{F}\mathbf{x}(k_i) - \boldsymbol{\Phi}_\omega\boldsymbol{\Delta}\boldsymbol{\omega}\right) + 2\boldsymbol{\Delta}\mathbf{U}\boldsymbol{\lambda}_u\mathbf{U}_\pi \quad (20)$$

IV. Simulation results

The optimization routine as described in the previous section was implemented using the MATLAB® Optimization Toolbox™. The model from (9) is implemented using C-code S-functions whereas the control algorithm is embedded into an M-code S-function.

In the following simulation results for the temperature control are shown to demonstrate the performance of the model predictive approach with regards to set-point changes but also to show the response of the closed loop due to disturbances as a result of possible weather changes. Furthermore, a comparison between a standard PI controller and the model predictive controller is made. The PI approach includes also feed-forward control to compensate for the system nonlinearities. This is to illustrate the benefits of the predictive approach regarding command response as well as the fact that effects such as the actuator saturation can be avoided. Furthermore, the maintenance of a defined comfort level by ensuring that the temperatures are within defined limits as well as a control taking the energy efficiency into account are further advantages of the model predictive control concept and therefore outweigh the performance of the standard PI controller significantly.

Figures 5 and 6 show the comparison regarding the temperature control at the output of the heat exchanger for the solar as well as the storage circuit using the model predictive controller as well as the standard PI controller.

The implementation of the model predictive control is carried out using a sample time of $1\,\mathrm{s}$ together with a prediction horizon N_p of $100\,\mathrm{s}$ and a control horizon N_c of $80\,\mathrm{s}$ where the constraints for the control variables $[0.1, 0.1]\,\mathrm{kg/s} \leq [\dot{m}_{sol}, \dot{m}_{sto}] \leq [1.7, 1.7]\,\mathrm{kg/s}$ and their rate of change $|\frac{\mathrm{d}}{\mathrm{d}t}[\dot{m}_{sol}, \dot{m}_{sto}]| \leq [0.03, 0.03]\,\mathrm{kg/s^2}$ must be satisfied. It can be clearly seen that the model predictive controller shows better performance regarding set-point changes showing

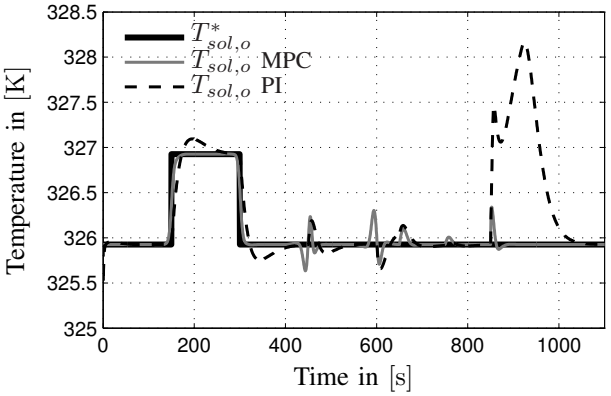

Fig. 5: Comparison MBPC vs. PI Temperature Control, Solar Circuit.

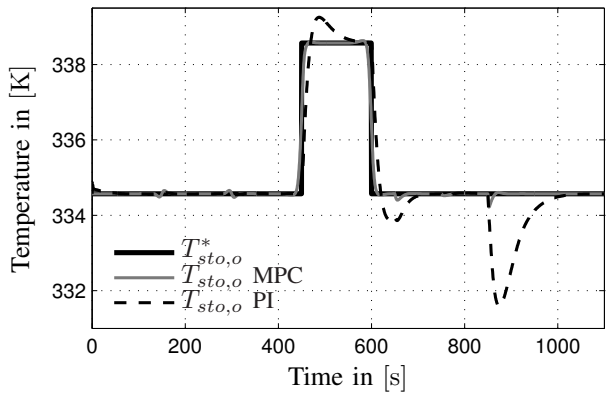

Fig. 6: Comparison MBPC vs. PI Temperature Control, Storage Circuit.

almost no overshoot and lower rise time due to its predictive behavior, see Figures 5 and 6. Constraints regarding the control variables are fulfilled perfectly well which is illustrated by Fig. 8.

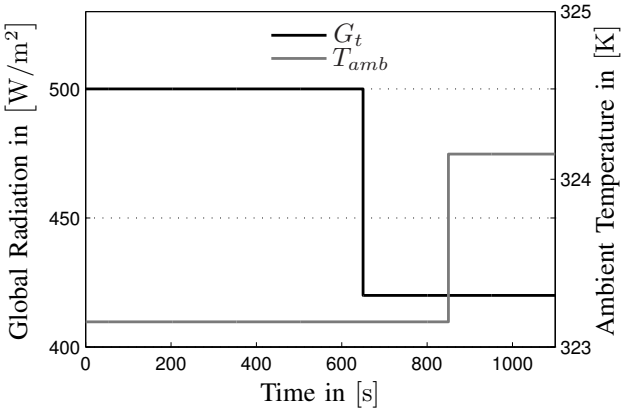

Fig. 7: Global solar radiation G_t and the ambient temperature T_{amb} as disturbances.

At time instants $650\,\mathrm{s}$ and $850\,\mathrm{s}$ (see Fig. 7) system dis-

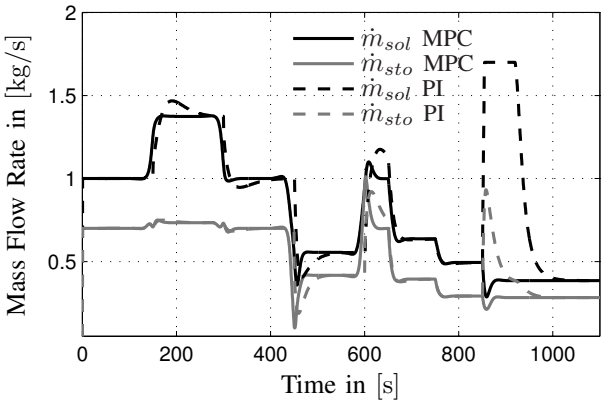

Fig. 8: Control Variables MBP vs PI Controller.

turbances due to change of radiation and inlet temperature in the storage circuit respectively are introduced to illustrate the performance of disturbance rejection where the model predictive controller shows a behavior with a much lower demand on control energy compared with the PI controller which even experiences actuator saturation at time $t = 860\,\mathrm{s}$ when trying to reject the rise of temperature at the inlet of the heat exchanger in the storage circuit $T_{sto,i}$, see Fig. 8. For this purpose an anti-windup method is applied to stop the integral action of the PI controller for the period of actuator saturation. Within the time period $t \in [0, 1100]\,\mathrm{s}$ the electric energy consumption can be reduced by approx. 19%. The consumed electric energy E_{elec} is calculated as a function of the time integral over simulation time $\tau = 1100\,\mathrm{s}$ of the sum of squared mass flow rates in the storage and the solar circuit assuming a linear pump characteristics:

$$E_{elec} \propto \int_0^{\tau} \left(\dot{m}_{sol}^2 + \dot{m}_{sto}^2\right) \mathrm{d}t \tag{21}$$

V. Conclusion

In this paper we proposed a model based predictive control concept for temperature control in the area of solar-thermal systems. We could show the great potential of the predictive approach regarding excellent response to set-point changes. Furthermore, the model predictive control strategy showed good performance with regards to disturbance rejections. The design of the model predictive controller is based on the minimization of the cost function also taking the electric energy consumption of the actuators into account. In order to underline the benefits we drew a comparison between the model predictive design and a standard PI controller. Thereby, we manage to reduce the energy consumption by approx. 19%. Future research will deal with simulations regarding longer time periods (e.g.: whole year) to obtain more detailed and comprehensive information on energy saving potentials when employing the discussed model based predictive control concept. Further, the effect of major variations of the global solar radiation on the robustness of the model predictive controller will be analyzed. Other works will deal with the employment of the nonlinear model predictive control for the solar-thermal system. Thereby, the solar-thermal system will then be extended by a stratified storage tank for which different energy cost functions to minimize for electric energy consumption of the actuators will be discussed.

References

[1] J. Laustsen, "Energy efficiency requirements in building codes, energy efficiency policies for new buildings," 2008, p. 10pp.

[2] L. Pérez-Lombard, J. Ortiz, and C. Pout, "A review on buildings energy consumption information," *Energy and Buildings*, vol. 40, no. 3, pp. 394–398, 2008.

[3] I. P. on Climate, *Climate Change 2007 - Mitigation of Climate Change: Working Group III Contribution to the Fourth Assessment Report of the IPCC*. Cambridge University Press, 2007.

[4] A. Steinboeck, K. Graichen, D. Wild, T. Kiefer, and A. Kugi, "Model-based trajectory planning, optimization, and open-loop control of a continuous slab reheating furnace," *Journal of Process Control*, 2010.

[5] G. Karer, G. Music, I. Skrjanc, and B. Zupancic, "Model predictive control of nonlinear hybrid systems with discrete inputs employing a hybrid fuzzy model," vol. 2, no. 2, 2008, pp. 491–509.

[6] A. Linder and R. Kennel, "Direct model predictive control - a new direct predictive control strategy for electrical drives," 2005.

[7] R. Balan, S. D. Stan, and C. Lapusan, "A model based predictive control algorithm for building temperature control," *3rd IEEE International Conference on Digital Ecosystems and Technologies*, pp. 540–545, 2009.

[8] F. Oldewurtel, A. Parisio, C. Jones, M. Morari, D. Gyalistras, M. Gwerder, V. Stauch, B. Lehmann, and K. Wirth, "Energy efficient building climate control using stochastic model predictive control and weather predictions," *American Control Conference (ACC)*, pp. 5100–5105, 2010.

[9] P. D. Morosan, R. Bourdais, D. Dumur, and J. Buisson, "Building temperature regulation using a distributed model predictive control," *Energy and Buildings*, vol. 42, no. 9, pp. 1445–1452, 2010.

[10] Z. Yu and A. Dexter, "Hierarchical fuzzy control of low-energy building systems," *Solar Energy*, vol. 84, no. 4, pp. 538–548, 2010.

[11] A. B. Nakhi and M. A. Mahmoud, "Energy conservation in buildings through efficient a/c control using neural networks," *Applied Energy*, vol. 73, no. 1, pp. 5–23, 2002.

[12] February 2011. [Online]. Available: http://www.energybase.at/

[13] February 2011. [Online]. Available: https://www.modelica.org/

[14] D. Basciotti, F. Dubisch, F. Fontanella, and F. Judex, "Modeling and validation of the energybase solar thermal collector field." EuroSun International Conference on Solar Heating, Cooling and Buildings, 2010.

[15] G. Fontanella, D. Basciotti, F. Dubisch, F. Judex, A. Preisler, C. Hettfleisch, V. Vukovic, and T. Selke, "Modeling and validation of the energybase solar thermal collector field." 8th International Conference on System Simulation in Buildings, 2010.

[16] G. Jonsson, "Modeling and parameter estimation of heat exchangers - a statistical approach," *Journal of Dynamic Systems, Measurement, and Control*, vol. 114, pp. 673–679, 1992.

[17] R. Shoureshi and H. M. Paynter, "Simple models for dynamics and control of heat exchangers," *American Control Conference*, pp. 1294–1298, 1983.

[18] G. Jonsson and O. P. Palsson, "Use of empirical relation in the parameters of heatexchager models," *Industrial and Engineering Chemistry Research*, vol. 30, no. 6, pp. 1193–1199, 1991.

[19] R. Zavala and R. Santiesteban-Cos, "Reliable compartmental models for double-pipe heat exchangers: An analytical study," *Applied Mathematical Modelling*, vol. 31, no. 9, pp. 1739–1752, 2007.

[20] S. A. Kalogirou, "Solar thermal collectors and applications," *Progress in Energy and Combustion Science*, vol. 30, no. 3, pp. 231–295, 2004.